


Real-time measurement of protein–protein interactions at single-molecule resolution using a biological nanopore

Avinash Kumar Thakur^{1,2} & Liviu Movileanu^{1–3} 

Protein–protein interactions (PPIs) are essential for many cellular processes. However, transient PPIs are difficult to measure at high throughput or in complex biological fluids using existing methods. We engineered a genetically encoded sensor for real-time sampling of transient PPIs at single-molecule resolution. Our sensor comprises a truncated outer membrane protein pore, a flexible tether, a protein receptor and a peptide adaptor. When a protein ligand present in solution binds to the receptor, reversible capture and release events of the receptor can be measured as current transitions between two open substates of the pore. Notably, the binding and release of the receptor by a protein ligand can be unambiguously discriminated in a complex sample containing fetal bovine serum. Our selective nanopore sensor could be applied for single-molecule protein detection, could form the basis for a nanoproteomics platform or might be adapted to build tools for protein profiling and biomarker discovery.

Physical associations between proteins (protein–protein interactions, PPIs) underpin cell functions in normal and pathogenic conditions and are important therapeutic targets¹. Existing methods detect transient PPIs at high spatial resolution using single-molecule technologies^{2–4}, but these methods are limited by low throughput. Conventional methods such as bilayer interferometry⁵ and surface plasmon resonance⁶ have been used in the affinity, kinetic and thermodynamic determinations of transient PPIs in bulk phase. Both are real-time techniques that can be used at high throughput. Surface plasmon resonance is limited by nonspecific protein binding on surfaces, surface heterogeneity, protein inactivation at the liquid–metal film interface, and molecular crowding effects. Isothermal titration calorimetry⁷ can report binding kinetics but is not high throughput and requires large quantities of proteins. Bilayer interferometry, surface plasmon resonance, and isothermal titration calorimetry provide average kinetic or affinity parameters and cannot be used in a heterogeneous sample.

Transient PPIs can be measured using a resistive-pulse technique⁸ and solid-state nanopores that are large enough to permit tethering of protein receptors on their internal surface^{9,10}. However, accurate identification of the anchoring site for tethered protein receptors remains difficult, which limits the sensitivity of single-molecule

measurements. An alternative approach to these shortcomings is the detection of reversible PPIs using an engineered protein nanopore. Protein nanopores have the advantage of being modifiable with atomic precision. Furthermore, sensing with engineered biological nanopores is amenable to integration into nanofluidic devices and high-throughput technologies¹¹. Biological nanopores could theoretically couple molecular precision with a parallel format^{12–16}.

Two requirements must be fulfilled to measure binding events between two folded proteins in solution using a protein nanopore. First, reversible PPIs must occur in the aqueous phase, because the dimensions of a protein–protein complex exceed the cross-sectional internal diameter of protein nanopores. Therefore, these interactions can only be detected outside the nanopore lumen^{17–19}. Second, a transducing mechanism is required to convert the reversible physical association and dissociation of the two interacting protein partners in the aqueous phase into a high-fidelity electrical signature of the nanopore sensor.

We report an engineered protein nanopore sensor that can detect reversible PPIs in solution and at single-tethered-receptor resolution. Because the detection of binding events occurs outside the lumen of the nanopore, we can apply our sensor to probe transient PPIs in mammalian serum. A single-polypeptide protein was created using t-FhuA²⁰, a monomeric β -barrel scaffold that is a truncated version of ferric hydroxamate uptake component A (FhuA)²¹ from *Escherichia coli* (**Fig. 1a**, top). A protein receptor (the 110-amino acid RNase barnase (Bn)²²) was fused to t-FhuA, on the β -turns side, with a flexible (GGG)₂ hexapeptide tether (Online Methods and **Supplementary Tables 1** and **2**). An H102A mutant of Bn was used because this lacks RNase activity^{22,23}, which in turn ensures that Bn-FhuA fusion proteins are not toxic to the expression host (Online Methods). The 455-residue t-FhuA scaffold formed a transmembrane pore²⁰, facilitating a quiet single-channel electrical signature for long periods when added to the *cis* side of the chamber (**Supplementary Fig. 1**). Both t-FhuA termini are accessible to the β -turns opening of the pore (**Fig. 1a**, top). We tested two protein pore nanostructures, in which Bn was fused to either the N terminus (Bn(GGG)₂t-FhuA) or the C terminus (t-FhuA(GGG)₂Bn) of t-FhuA. The average single-channel conductance noted with t-FhuA was 1.6 ± 0.1 nS ($n = 6$) at a transmembrane potential of -40 mV and in 300 mM KCl, 10 mM Tris-HCl, pH 8 (**Supplementary Fig. 1**). Bn(GGG)₂t-FhuA and

¹Department of Physics, Syracuse University, Syracuse, New York, USA. ²Structural Biology, Biochemistry, and Biophysics Program, Syracuse University, Syracuse, New York, USA. ³Department of Biomedical and Chemical Engineering, Syracuse University, Syracuse, New York, USA. Correspondence should be addressed to L.M. (lmovilea@syr.edu).

Received 10 January; accepted 11 November; published online 10 December 2018; doi:10.1038/nbt.4316

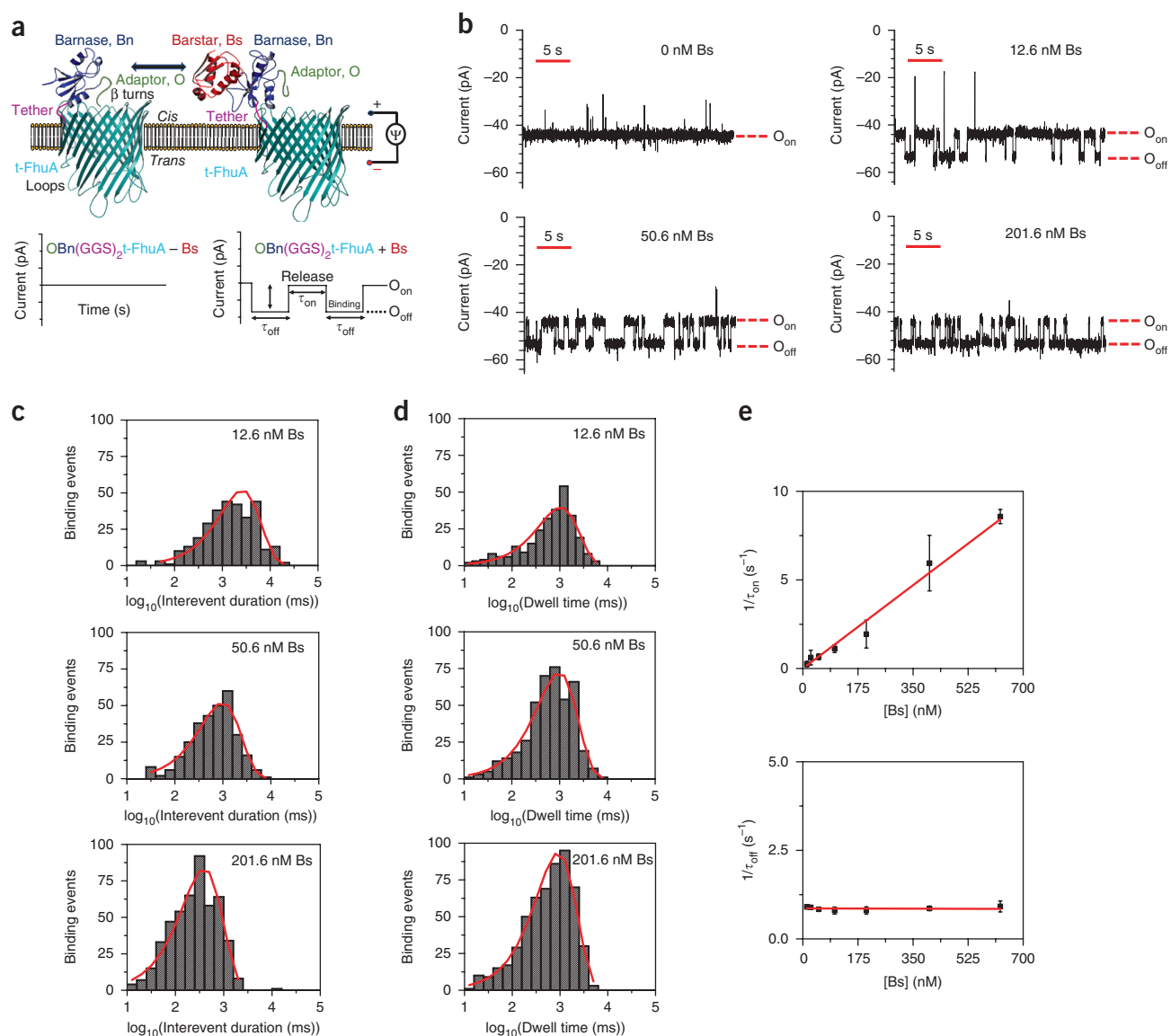


Figure 1 Measuring high-affinity PPIs using a nanopore sensor. **(a)** Top, a protein pore-based nanostructure for the real-time sampling of transient PPIs. The single-polypeptide protein comprises a t-FhuA protein pore scaffold, a flexible (GGG)₂ tether, a barnase (Bn) protein receptor and an O peptide adaptor. The schematic model was created in PyMol using the Protein Data Bank files 1BY3 (FhuA)²¹ and 1BRS (Bn–Bs)³⁴. Bottom, stochastic sensing of transient PPIs using a single OBn(GGS)₂t-FhuA protein. The protein nanostructure maintains a basal open-state conductance (left). When added to the *cis* side, the Bs protein ligand is expected to produce current transitions between two conductance substates (right). **(b)** Reversible captures of tethered Bn by Bs were observed through well-defined current transitions. Bs was added to the *cis* compartment. O_{on} represents the Bn-released open substate; O_{off} represents the Bn-captured open substate. This single-channel electrical signature was replicated in three independent experiments. The applied transmembrane potential was -40 mV. Single-channel electrical traces were further low-pass eight-pole Bessel filtered at 100 Hz. **(c)** Representative semilogarithmic histograms of the interevent duration (τ_{on}) of the transient PPIs at various Bs concentrations. The τ_{on} duration (mean \pm s.e.m.) was 2,338 \pm 236 ms (number of events: $n = 302$), 1,312 \pm 102 ms ($n = 300$), and 458 \pm 15 ms ($n = 481$) at Bs concentrations of 12.6 nM, 50.6 nM and 201.6 nM, respectively. **(d)** Representative semilogarithmic event dwell-time (τ_{off}) histograms of the PPIs at various Bs concentrations. The τ_{off} dwell times (mean \pm s.e.m.) determined from these histograms were 1,142 \pm 78 ms ($n = 278$ events), 1,155 \pm 72 ms ($n = 424$), and 1,085 \pm 57 ms ($n = 547$) at Bs concentrations of 12.6 nM, 50.6 nM and 201.6 nM, respectively. **(e)** Diagrams illustrating the dependence of $1/\tau_{on}$ and $1/\tau_{off}$ on the Bs concentration. The slope of the linear fit of $1/\tau_{on}$ versus the Bs concentration [Bs], is the association rate constant, k_{on} , of the PPIs because $k_{on} = 1/(\tau_{on}[Bs])$. The horizontal line is an average fit of the ($1/\tau_{off}$) data points recorded for various [Bs] values. Data points in both panels represent mean \pm s.d. obtained from $n = 3$ distinct experiments.

t-FhuA(GGS)₂Bn showed average single-channel conductance values that were similar to that recorded with t-FhuA. Bn(GGS)₂t-FhuA and t-FhuA(GGS)₂Bn also exhibited stability of the open-state current for long periods. These results suggest that Bn is located outside the pore lumen, on the β -turns side of t-FhuA. Moreover, these findings

indicate that t-FhuA tolerates large polypeptide extensions at either terminus without affecting its pore-forming ability.

The protein ligand we used in our initial set of measurements was the 89-residue barstar (Bs)²⁴, which is an inhibitor of Bn RNase activity. Surprisingly, the addition of 201.6 nM Bs to the *cis* side,

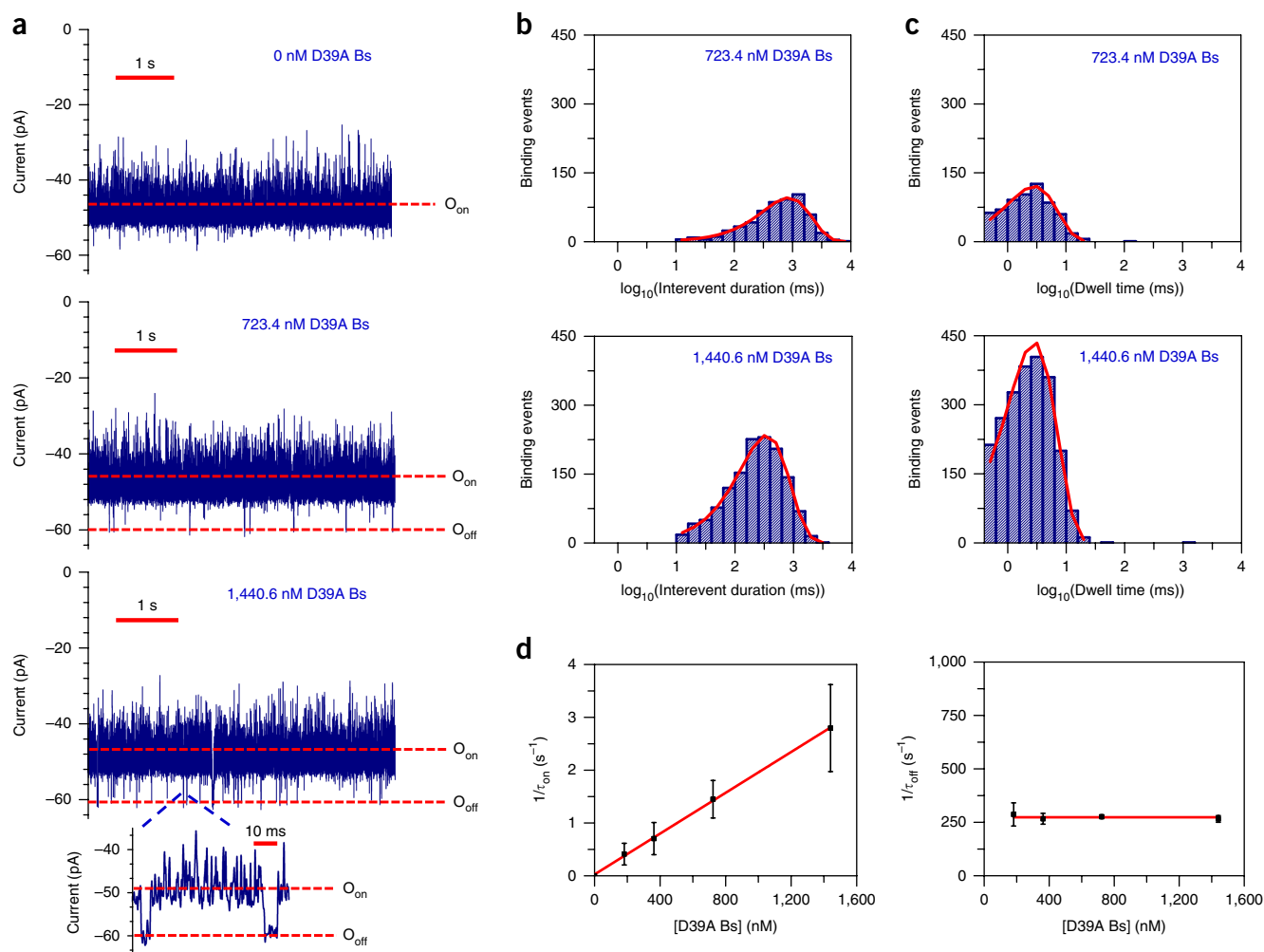


Figure 2 Measuring low-affinity PPIs using a nanopore sensor. **(a)** Representative single-molecule captures of transient PPIs between Bn and D39A Bs using OBn(GGS)₂t-FhuA. This single-channel electrical signature was replicated in three independent experiments. The applied transmembrane potential was -40 mV. The low-affinity D39A Bs was added to the *cis* compartment. The current traces were low-pass Bessel filtered at 1 kHz. **(b)** Representative semi-logarithmic histograms of the interevent duration, τ_{on} , of the PPIs at two D39A Bs concentrations. The τ_{on} values (mean \pm s.e.m.) were 855 ± 1 (number of events: $n = 560$) and 378 ± 12 ms ($n = 1,349$) at D39A Bs concentrations of 723.4 nM and 1,440.6 nM, respectively. **(c)** Representative semilogarithmic event dwell-time histograms of the weak PPIs at two D39A Bs concentrations. The τ_{off} values (mean \pm s.e.m.) determined from these histograms were 3.6 ± 0.2 ms ($n = 622$ events) and 3.6 ± 0.1 ms ($n = 2,240$) at a D39A Bs concentration of 723.4 nM and 1,440.6 nM, respectively. **(d)** Diagrams illustrating the dependence of $1/\tau_{on}$ and $1/\tau_{off}$ on the D39A Bs concentration. The slope of the linear fit of $1/\tau_{on}$ versus [D39A Bs] is the association rate constant, k_{on} , of the PPIs. The bottom diagram shows that the τ_{off} binding time was independent of the D39A Bs concentration. Data points in both panels represent mean \pm s.d. obtained from either $n = 3$ (723.4 nM and 1,440.6 nM) or $n = 4$ (181.4 nM and 362.4 nM) distinct experiments.

either with reconstituted Bn(GGS)₂t-FhuA or with t-FhuA(GGS)₂Bn, failed to produce reversible alterations in the electrical signature (**Supplementary Fig. 2**). It is possible that the Bn receptor adopts a conformation that blocks the accessibility of its binding site to Bs, or that Bn–Bs interactions in solution are indistinguishable (electrically silent) in the readout. We favor the hypothesis that Bn does not obstruct ionic flux through the pore, and that transient Bn–Bs complex formation pulls Bn away from the pore opening. This hypothesis relies on single-channel measurements using t-FhuA, whose electrical signature is indistinguishable from those recorded either with Bn(GGS)₂t-FhuA or t-FhuA(GGS)₂Bn (**Supplementary Fig. 1**).

To obtain an altered single-channel electrical signature of Bn(GGS)₂t-FhuA that might be sensitive to Bn–Bs specific interactions,

we fused a 12-residue peptide adaptor (O) to the N terminus of Bn, resulting in OBn(GGS)₂t-FhuA (**Fig. 1a**, top, and **Supplementary Fig. 3a**). Our peptide adaptor has an unstructured and slightly negatively charged sequence²⁵ that should span the distance between the N terminus of Bn (its fusion point) and the pore opening. This distance is ~ 4 nm, assuming that the flexible (GGS)₂ linker is extended. We hypothesized that this peptide adaptor would exhibit nonspecific interactions with the highly acidic entrance of the pore, resulting in a distinct and sensitive electrical signature. We found that OBn(GGS)₂t-FhuA had a reduced unitary conductance of 1.23 ± 0.03 nS ($n = 8$) at a transmembrane potential of -40 mV (**Supplementary Fig. 3b,c**). Further, OBn(GGS)₂t-FhuA exhibited frequent, brief, and upwards current spikes (**Supplementary Figs. 4 and 5**). The fusion of the peptide adaptor to the N terminus of Bn(GGS)₂t-FhuA likely induces an

obstruction moiety near the pore opening of t-FhuA, thereby reducing its unitary conductance.

Remarkably, when Bs was added to the *cis* side in the nanomolar range, we detected reversible current transitions between O_{on} , a lower-current-amplitude open substate, and O_{off} , a higher-current-amplitude open substate (Fig. 1a, bottom, Fig. 1b and Supplementary Table 3). We interpret these current transitions as reversible capture (O_{off}) and release (O_{on}) events of Bn by Bs. We hypothesize that the transient capture events are accompanied by pulling the obstruction moiety away from the pore opening, increasing the open-state current to O_{off} . This level is closely similar to that noted with Bn(GGS)₂t-FhuA (Supplementary Fig. 3b). This interpretation is in accord with a quieter and higher-conductance open substate of the capture events (Supplementary Figs. 4 and 6).

The current amplitudes of O_{off} and O_{on} enabled an unambiguous separation of the 'off' (quiet substate) and 'on' (noisy substate) events, with a difference of 10 ± 2 pA ($n = 3$). Notably, reversible current transitions were only observed when Bs was added to the *cis* side, but not to the *trans* side (Supplementary Fig. 7), which confirmed that the truncated FhuA protein pores insert into the lipid bilayer with a preferred orientation^{26,27}. The pore is inserted such that the loops face the *trans* side and the β turns face the *cis* side (Fig. 1a, top)²⁰.

Next we tested the single-molecule kinetics of the Bn–Bs interactions and found that the frequency of Bn–Bs binding events increased with Bs concentration (Fig. 1b). Semilogarithmic representations of the interevent duration, τ_{on} , and dwell time, τ_{off} , analyses are shown in Figure 1c and Figure 1d, respectively. Note that the center location of the peak is the logarithm of the time constant. The standard interevent duration and dwell-time analyses of the 'on' and 'off' events are illustrated in Supplementary Figures 8 and 9, respectively. We applied a logarithm likelihood ratio test to fit models of these histograms (Fig. 1c,d), and this showed that 'on' and 'off' events had a single-exponential-value distribution, suggesting a single-barrier transition of the free-energy landscape of these PPIs.

The frequency of the Bn–Bs binding events in the form of $1/\tau_{on}$ was linearly dependent on the Bs concentration, confirming a bimolecular association process (Fig. 1e). The slope of the linear fit of event frequency was the association rate constant k_{on} . The reciprocal of the τ_{off} duration, which is the dissociation rate constant k_{off} , was independent of the Bs concentration, confirming a unimolecular dissociation process. We obtained $k_{on} = (1.34 \pm 0.04) \times 10^7 \text{ M}^{-1}\text{s}^{-1}$ and $k_{off} = 0.86 \pm 0.02 \text{ s}^{-1}$, corresponding to an equilibrium dissociation constant K_d of $64 \pm 02 \text{ nM}$ (Supplementary Table 4). The value of this constant indicated a high-affinity PPI of the Bn–Bs pair. This agrees well with previous kinetic measurements of Bn–Bs interactions^{22,23}. Furthermore, we found that the signal-to-noise ratio was not increased by an increase in Bs concentration, even in the low micromolar range (Supplementary Fig. 10). At higher Bs concentrations, the frequency of PPI events showed a nonlinear dependence on protein concentration, likely owing to saturation of the Bn binding site (Supplementary Fig. 11).

Weak PPIs, with K_d values in the micromolar or millimolar range, are important in many signaling pathways²⁸. The main difficulty in detecting weak PPIs is either high-dissociation or low-association rate constants, or both². To test the ability of OBn(GGS)₂t-FhuA to detect weaker PPIs, we carried out single-channel recordings using D39A Bs, a Bs variant with greatly reduced binding affinity to Bn. When a low-nanomolar concentration of D39A Bs was added to the *cis* side, reversible current transitions occurred between O_{on} and O_{off} , but with a binding duration in the low-millisecond range. τ_{off} was much shorter than the value for the Bn–Bs pair (Fig. 2a). This weak

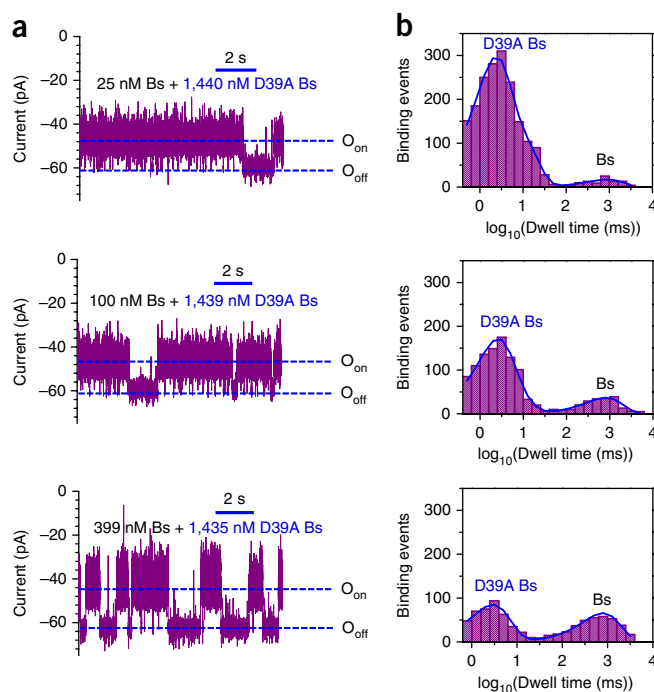


Figure 3 Concurrent detection of weak and strong PPIs using a nanopore sensor. (a) Representative single-channel current traces of OBn(GGS)₂ t-FhuA were collected at an applied transmembrane potential of -40 mV when different mixtures of protein ligands were added to the *cis* compartment: (i) 1,440 nM D39A Bs and 25 nM Bs (top trace); (ii) 1,439 nM D39A Bs and 100 nM Bs (middle trace); (iii) 1,435 nM D39A Bs and 399 nM Bs (bottom trace). These single-channel electrical signatures were replicated in three independent experiments. The single-channel electrical traces were low-pass Bessel filtered at 1 kHz. (b) Representative event dwell-time histograms of the weak and strong PPIs: (i) 1,440 nM D39A Bs and 25 nM Bs (top diagram); (ii) 1,439 nM D39A Bs and 100 nM Bs (middle diagram); (iii) 1,435 nM D39A Bs and 399 nM Bs (bottom diagram). The average τ_{off} dwell times (mean \pm s.e.m.), which corresponded to D39A Bs and Bs, respectively, were the following: (i) 4.1 ± 0.1 ms and 904 ± 1 ms ($n = 1,888$ events; top diagram); (ii) 3.4 ± 0.1 ms and 829 ± 1 ms ($n = 1,153$; middle diagram); (iii) 3.3 ± 0.1 ms and 827 ± 1 ms ($n = 789$; bottom diagram).

interaction had interevent duration (Fig. 2b) and dwell-time (Fig. 2c) histograms with single-exponential distributions. The standard interevent duration and dwell-time analyses of the corresponding 'on' and 'off' events are reported in Supplementary Figures 12 and 13, respectively. τ_{on} decreased when D39A Bs concentration was increased (Supplementary Table 5) whereas there was no statistically significant alteration in τ_{off} when D39A Bs concentration was changed. The frequency of low-affinity events increased linearly with increasing the D39A Bs concentration, consistent with our results using high-affinity binder Bs (Fig. 2d). Our finding of $k_{on} = (0.193 \pm 0.003) \times 10^7 \text{ M}^{-1}\text{s}^{-1}$ and $k_{off} = 281 \pm 8 \text{ s}^{-1}$, to yield a K_d of $146 \pm 4 \mu\text{M}$ (Supplementary Table 4), is consistent with earlier studies carried out in bulk phase²³. For example, in 50 mM Tris-HCl, pH 8, transient PPIs between Bn and D39A Bs had k_{off} and K_d values of $\sim 17 \text{ s}^{-1}$ and $\sim 39 \text{ nM}$, respectively. These PPIs are about two orders of magnitude weaker than those recorded for Bn and Bs, which had a K_d of $\sim 0.32 \text{ nM}$ in the same conditions. This shows that our nanopore sensor can detect transient PPIs at protein ligand concentrations several orders of magnitude below the measured K_d . Transient PPIs cannot easily be measured at millisecond-time resolution with other biophysical

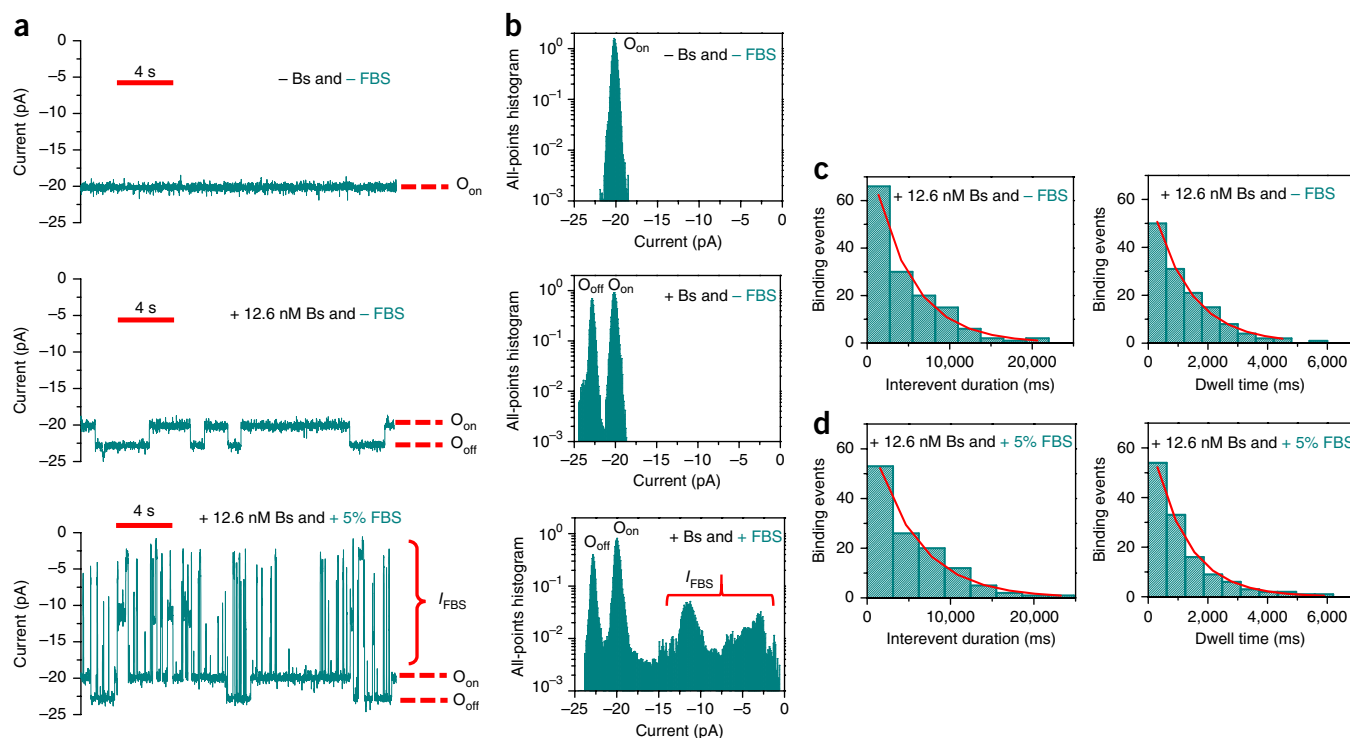


Figure 4 Single-molecule protein detection and observation of transient PPIs using a nanopore sensor in FBS. **(a)** Representative single-molecule binding events of the Bn–Bs pair using OBn(GGS)₂t-FhuA in 5% (v/v) FBS at an applied transmembrane potential of –15 mV. This single-channel electrical signature was replicated in three independent experiments. Single-channel electrical traces were low-pass Bessel filtered at 40 Hz. **(b)** Representative all-points histograms for the duration of the displayed single-channel electrical traces in **a**. This single-channel electrical signature was replicated in three independent experiments. **(c)** Representative histograms of the interevent durations (τ_{on}) and the event dwell times (τ_{off}) at 12.6 nM Bs and in the absence of FBS. The τ_{on} and τ_{off} durations (mean \pm s.e.m.) determined from these fits were $5,182 \pm 200$ ms ($n = 140$ events) and $1,272 \pm 53$ ms ($n = 133$), respectively. **(d)** Representative histograms of the interevent durations (τ_{on}) and the event dwell times (τ_{off}) for the Bn–Bs interactions at 12.6 nM Bs and in the presence of 5% (v/v) FBS. The τ_{on} and τ_{off} durations (mean \pm s.e.m.) determined from these histogram fits were $5,153 \pm 299$ ms (number of events: $n = 120$) and $1,165 \pm 54$ ms ($n = 127$), respectively.

methods in solution²⁸ whereas our nanopore sensor shows promise for detecting weak PPIs with high k_{off} values.

An ability to detect multiple analytes in a mixture of proteins is needed for diagnostic applications, and we next tested whether our sensor could identify low- and high-affinity PPIs in a mixture. When both Bs and D39A Bs were added, we detected both long-lived and brief transitions (Fig. 3a,b and Supplementary Tables 6 and 7). Increasing the concentration of high-affinity Bs resulted in an increase in the frequency of long-lived current transitions and a reduction in the frequency of the brief binding events. These experiments revealed that our nanopore sensor can discriminate competitive interactions between two Bs variants for the same binding site.

We also tested whether our sensor could detect Bs in the presence of fetal bovine serum (FBS). In the absence of Bs, OBn(GGS)₂t-FhuA exhibited a uniform and quiet unitary current at a transmembrane potential of –15 mV ($n = 3$; Fig. 4a, upper trace). Single-channel traces acquired with OBn(GGS)₂t-FhuA in the presence of 12.6 nM Bs, which was added to the *cis* side, displayed reversible low-current amplitude transitions between O_{on} and O_{off} ($n = 3$; Fig. 4a, middle trace). In the presence of 5% (v/v) FBS, large-amplitude current blockades were recorded, more than likely produced by serum constituents that partitioned into the pore lumen ($n = 3$; I_{FBS} ; Fig. 4a, bottom trace). However, the single-channel electrical traces also showed low-amplitude, PPIs-induced current transitions that were unambiguously distinguished from large-amplitude current blockades ($n = 3$; Fig. 4b).

We chose a voltage of –15 mV because at a greater transmembrane potential of –40 mV the FBS-produced current blockades were very long (Supplementary Fig. 14). These long-lived blockades precluded a precise evaluation of the kinetic rate constants. Notably, the transient PPIs recorded at transmembrane potentials of –15 and –40 mV displayed no statistically significant distinctions in kinetic rate constants (Supplementary Tables 3, 4 and 8).

Representative standard histograms acquired in the absence and presence of 5% (v/v) FBS are displayed in Figure 4c and Figure 4d, respectively. Notably, k_{on} and k_{off} values of the transient PPI in the absence and presence of FBS were similar (Supplementary Table 8). To test the sensitivity of our single-molecule sensor, we determined the Bs concentration in the presence of FBS using $C_{Bs} = 1/(\tau_{on}k_{on})$, where C_{Bs} , τ_{on} and k_{on} are the concentration of the sampled Bs protein, interevent duration determined in the presence of FBS, and association rate constant inferred for Bs in the absence of FBS, respectively. The average Bs concentration was 13.3 ± 5.0 nM ($n = 3$). This value is in agreement with the actual Bs concentration added to the *cis* chamber (12.6 nM Bs). Therefore, our nanopore sensor can detect and quantify a protein analyte in a complex biological fluid. Further, we were able to obtain detailed kinetic information of the transient PPIs even in these challenging conditions.

Most biophysical approaches for the quantification of kinetics of transient PPIs are carried out in bulk phase and report average measurements of an ensemble of proteins in solution. In contrast,

our method has the potential to detect and characterize subpopulations of distinct binding events in a complex biofluid environment. Furthermore, our genetically encoded sensor shows promise for the identification of rare and brief binding events, which to our knowledge cannot be detected using existing technologies. We also anticipate that temperature-dependent electrical recordings might be able to illuminate enthalpic and entropic contributions to kinetic rate constants of association and dissociation of transient PPIs. Simultaneous determination of the k_{off} values for more than one protein target, while providing the apparent k_{on} and half-maximal inhibitory concentration values, is quite a challenging task employing other techniques in solution. Using our single-molecule nanopore sensor, we were able to examine competitive protein interactions with the same binding site. We have shown that our nanopore sensor can probe k_{off} in the range of 10^2 – 10^3 s⁻¹. There is no theoretical reason to suggest that our sensor could not resolve even shorter PPIs events that have even faster dissociation rate constants, such as extremely weak PPIs involved in the rapid responses of cell signaling².

Because our sensor is genetically encoded, we envisage that it could form the basis of a combinatorial sensor library of different protein receptors with potential application in clinical nanoproteomics, or high-throughput screening of small-molecule drugs or peptide inhibitors. Finally, the ability to distinguish a specific PPI in a complex biological fluid sample reveals the potential of this sensor for single-molecule protein detection^{29–33} in cell lysates, biopsies or blood.

METHODS

Methods, including statements of data availability and any associated accession codes and references, are available in the [online version of the paper](#).

Note: Any Supplementary Information and Source Data files are available in the [online version of the paper](#).

ACKNOWLEDGMENTS

We thank S. Loh for generosity in using his FPLC instrument in the very early stages of these studies and A. Matouschek (University of Texas at Austin) for his kindness in offering plasmids containing genes that encode Bn and Bs proteins, as well as M.L. Ghahari and M.M. Mohammad for their assistance in the very early stages of this project. This work was supported by US National Institutes of Health grants GM088403 (L.M.) and GM129429 (L.M.).

AUTHOR CONTRIBUTIONS

A.K.T. and L.M. designed research. A.K.T. performed research and analyzed data. A.K.T. and L.M. wrote the paper.

COMPETING INTERESTS

A.K.T. and L.M. are named inventors on two provisional patent applications (US 62/720,190 and US 62/579,982) filed by Syracuse University on this work.

Reprints and permissions information is available online at <http://www.nature.com/reprints/index.html>. Publisher's note: Springer Nature remains neutral with regard to jurisdictional claims in published maps and institutional affiliations.

- Hayes, S., Malacrida, B., Kiely, M. & Kiely, P.A. Studying protein-protein interactions: progress, pitfalls and solutions. *Biochem. Soc. Trans.* **44**, 994–1004 (2016).
- Yoo, J., Lee, T.S., Choi, B., Shon, M.J. & Yoon, T.Y. Observing extremely weak protein-protein interactions with conventional single-molecule fluorescence microscopy. *J. Am. Chem. Soc.* **138**, 14238–14241 (2016).
- De Keersmaecker, H. *et al.* Mapping transient protein interactions at the nanoscale in living mammalian cells. *ACS Nano* **12**, 9842–9854 (2018).
- Nogal, B., Bowman, C.A. & Ward, A.B. Time-course, negative-stain electron microscopy-based analysis for investigating protein-protein interactions at the single-molecule level. *J. Biol. Chem.* **292**, 19400–19410 (2017).
- Gonzalez, L.C. Protein microarrays, biosensors, and cell-based methods for secretome-wide extracellular protein-protein interaction mapping. *Methods* **57**, 448–458 (2012).
- Douzi, B. Protein-protein interactions: surface plasmon resonance. *Methods Mol. Biol.* **1615**, 257–275 (2017).
- Pierce, M.M., Raman, C.S. & Nall, B.T. Isothermal titration calorimetry of protein-protein interactions. *Methods* **19**, 213–221 (1999).
- Sackmann, B. & Neher, E. *Single-Channel Recording*. Second edn. (Kluwer Academic/Plenum, New York, 1995).
- Wei, R., Gatterdam, V., Wieneke, R., Tampé, R. & Rant, U. Stochastic sensing of proteins with receptor-modified solid-state nanopores. *Nat. Nanotechnol.* **7**, 257–263 (2012).
- Ying, Y.L., Yu, R.J., Hu, Y.X., Gao, R. & Long, Y.T. Single antibody-antigen interactions monitored via transient ionic current recording using nanopore sensors. *Chem. Commun. (Camb.)* **53**, 8620–8623 (2017).
- Weichbrodt, C. *et al.* Antibiotic translocation through porins studied in planar lipid bilayers using parallel platforms. *Analyst* **140**, 4874–4881 (2015).
- Reiner, J.E. *et al.* Disease detection and management via single nanopore-based sensors. *Chem. Rev.* **112**, 6431–6451 (2012).
- Deamer, D., Akeson, M. & Branton, D. Three decades of nanopore sequencing. *Nat. Biotechnol.* **34**, 518–524 (2016).
- Ayub, M. & Bayley, H. Engineered transmembrane pores. *Curr. Opin. Chem. Biol.* **34**, 117–126 (2016).
- Burns, J.R., Seifert, A., Fertig, N. & Howorka, S. A biomimetic DNA-based channel for the ligand-controlled transport of charged molecular cargo across a biological membrane. *Nat. Nanotechnol.* **11**, 152–156 (2016).
- Howorka, S. Building membrane nanopores. *Nat. Nanotechnol.* **12**, 619–630 (2017).
- Movileanu, L., Howorka, S., Braha, O. & Bayley, H. Detecting protein analytes that modulate transmembrane movement of a polymer chain within a single protein pore. *Nat. Biotechnol.* **18**, 1091–1095 (2000).
- Rotem, D., Jayasinghe, L., Salichou, M. & Bayley, H. Protein detection by nanopores equipped with aptamers. *J. Am. Chem. Soc.* **134**, 2781–2787 (2012).
- Harrington, L., Cheley, S., Alexander, L.T., Knapp, S. & Bayley, H. Stochastic detection of Pim protein kinases reveals electrostatically enhanced association of a peptide substrate. *Proc. Natl. Acad. Sci. USA* **110**, E4417–E4426 (2013).
- Thakur, A.K., Larimi, M.G., Gooden, K. & Movileanu, L. Aberrantly large single-channel conductance of polyhistidine arm-containing protein nanopores. *Biochemistry* **56**, 4895–4905 (2017).
- Locher, K.P. *et al.* Transmembrane signaling across the ligand-gated FhuA receptor: crystal structures of free and ferrichrome-bound states reveal allosteric changes. *Cell* **95**, 771–778 (1998).
- Schreiber, G. & Fersht, A.R. Interaction of barnase with its polypeptide inhibitor barstar studied by protein engineering. *Biochemistry* **32**, 5145–5150 (1993).
- Schreiber, G. & Fersht, A.R. Energetics of protein-protein interactions: analysis of the barnase-barstar interface by single mutations and double mutant cycles. *J. Mol. Biol.* **248**, 478–486 (1995).
- Deyev, S.M., Waibel, R., Lebedenko, E.N., Schubiger, A.P. & Plückthun, A. Design of multivalent complexes using the barnase*barstar module. *Nat. Biotechnol.* **21**, 1486–1492 (2003).
- Kudlinzki, D., Schmitt, A., Christian, H. & Ficner, R. Structural analysis of the C-terminal domain of the spliceosomal helicase Prp22. *Biol. Chem.* **393**, 1131–1140 (2012).
- Mohammad, M.M., Howard, K.R. & Movileanu, L. Redesign of a plugged beta-barrel membrane protein. *J. Biol. Chem.* **286**, 8000–8013 (2011).
- Mohammad, M.M. *et al.* Engineering a rigid protein tunnel for biomolecular detection. *J. Am. Chem. Soc.* **134**, 9521–9531 (2012).
- Perkins, J.R., Diboun, I., Dessailly, B.H., Lees, J.G. & Orenco, C. Transient protein-protein interactions: structural, functional, and network properties. *Structure* **18**, 1233–1243 (2010).
- Nivala, J., Mulrone, L., Li, G., Schreiber, J. & Akeson, M. Discrimination among protein variants using an unfoldase-coupled nanopore. *ACS Nano* **8**, 12365–12375 (2014).
- Kennedy, E., Dong, Z., Tennant, C. & Timp, G. Reading the primary structure of a protein with 0.07 nm³ resolution using a subnanometre-diameter pore. *Nat. Nanotechnol.* **11**, 968–976 (2016).
- Sze, J.Y.Y., Ivanov, A.P., Cass, A.E.G. & Edl, J.B. Single molecule multiplexed nanopore protein screening in human serum using aptamer modified DNA carriers. *Nat. Commun.* **8**, 1552 (2017).
- Huang, G., Willems, K., Soskine, M., Wloka, C. & Maglia, G. Electro-osmotic capture and ionic discrimination of peptide and protein biomarkers with FraC nanopores. *Nat. Commun.* **8**, 935 (2017).
- Restrepo-Pérez, L., Joo, C. & Dekker, C. Paving the way to single-molecule protein sequencing. *Nat. Nanotechnol.* **13**, 786–796 (2018).
- Buckle, A.M., Schreiber, G. & Fersht, A.R. Protein-protein recognition: crystal structural analysis of a barnase-barstar complex at 2.0-Å resolution. *Biochemistry* **33**, 8878–8889 (1994).

ONLINE METHODS

Design and mutagenesis of the expression constructs. All of the designed genes were constructed using conventional and assembly PCR techniques, and cloned into the expression vector pPR-IBA1 using respective restriction sites. *bn(ggs)₂t-fhua*, which encodes barnase (Bn)³⁴ at the N terminus of the heavily truncated t-FhuA protein²⁰ via a flexible glycine- and serine-rich tether and BsaI site, was prepared from the *bn* and *t-fhua* genes using three PCR reactions. The first PCR reaction was performed using *bn* as a template DNA, the forward primer (1) (Supplementary Table 1) and reverse primer (2). The second PCR reaction was performed using *t-fhua* as a template DNA, with the forward primer (3) and reverse primer (4). The third PCR reaction was performed using PCR 1 and PCR 2 products as a template DNA, with the forward primer (1) and reverse primer (4). *obn[ggs]₂t-fhua*, which encoded the peptide adaptor, O, MGDRGPEFELGT, fused to the N terminus of Bn; a flexible glycine- and serine-rich tether; t-FhuA; and a KpnI site at the 5' and 3' ends, was prepared from the *bn* and *t-fhua* genes via three PCR reactions. The first PCR reaction was performed using *bn* as a template DNA, along with the forward primer (5) and reverse primer (6). For the second PCR reaction, *t-fhua* was used as a template DNA, with the forward primer (7) and reverse primer (4). The third PCR reaction was performed using PCR 1 and PCR 2 products as a template DNA, with the forward primer (5) and reverse primer (4). The *bs* gene encoded the barstar (Bs) protein ligand. We removed all the purification tags from the plasmid (plasmid courtesy of Andreas Matouschek) using the forward primer (8) and reverse primer (9), then subcloned it into the pPR-IBA1 expression vector using BsaI restriction sites. The *bs* gene also encoded a double alanine mutant, C40A/C82A (ref. 35). The gene encoding D39A Bs was prepared by performing an inverse PCR using the forward primer (10) and reverse primer (11).

Protein expression and purification. All of the constructed genes were transformed into *E. coli* BL21(DE3) cells for protein expression. Bn(GGS)₂-FhuA, t-FhuA(GGS)₂Bn and OBn(GGS)₂-FhuA were expressed and purified as previously described²⁰. In the case of Bs and D39A Bs, transformed cells were grown in Luria-Bertani medium at 37 °C until OD₆₀₀ reached a value of ~0.5, after which the temperature was changed to 20 °C. Bs expression was initiated by inducing the cells with IPTG when OD₆₀₀ was ~0.7. After induction, the cells were further cultured for another ~18 h at 20 °C. Then the cells were centrifuged at 3,700g for 30 min at 4 °C, followed by their resuspension in 150 mM KCl, 50 mM Tris-HCl, 5 mM EDTA, pH 8. The cell lysis was accomplished using a Model 110L microfluidizer (Microfluidics, Newton, MA). Cell lysates were centrifuged at 108,500g for 30 min at 4 °C to separate the insoluble pellet and supernatant. The supernatant was further processed for ammonium sulfate precipitation. In the first step, ammonium sulfate was slowly dissolved into the supernatant to a final concentration of 10% (w/v) at 4 °C for 30 min. Next the supernatant was centrifuged at 108,500g for 30 min at 4 °C to separate the precipitate and supernatant. The supernatant was then processed as in the previous step with 40% ammonium sulfate. The collected supernatant was dialyzed extensively against 20 mM Tris-HCl, pH 8, overnight at 4 °C. Dialyzed supernatant was then purified on a Q-Sepharose column (Bio-Rad, Hercules, CA) using a linear salt gradient of 0–1 M KCl, 20 mM Tris-HCl, pH 8.

Pure fractions were further passed through the Superdex-75 size-exclusion column (SEC; GE Healthcare Life Sciences, Pittsburgh, PA) as a refining purification step. Pure Bs variants were stored at –80 °C. Protein purity was tested by SDS–PAGE analysis.

Protein refolding. Lyophilized Bn(GGS)₂-FhuA, t-FhuA(GGS)₂Bn and OBn(GGS)₂-FhuA were solubilized in 200 mM KCl, 8 M urea, 50 mM Tris-HCl, pH 8 to a final concentration of ~15 μM and incubated at room temperature for at least 4 h before refolding. Next, *n*-dodecyl-β-D-maltopyranoside (DDM) was added to denatured samples to a final concentration of 1.5% (w/v). The protein samples were immediately dialyzed against the buffer containing 200 mM KCl, 20 mM Tris-HCl, pH 8, at 4 °C for a duration of at least 72 h. Then the refolded protein samples were diluted 20-fold in 200 mM KCl, 20 mM Tris-HCl, pH 8, 0.5% DDM before single-channel electrical recordings. Protein concentrations were determined by their molar absorptivity at a wavelength of 280 nm.

Single-channel electrical recordings using planar lipid bilayers. Single-molecule electrophysiology measurements employed planar lipid bilayers, as previously reported²⁶. The proteins were added to the *cis* compartment, which was at ground, to a final concentration ranging between 0.3 and 1 ng/μl. Single-channel electrical currents were acquired using an Axopatch 200B patch-clamp amplifier (Axon Instruments, Foster City, CA). For all experiments, the electrolyte solution contained 300 mM KCl, 10 mM Tris-HCl, pH 8. Single-channel current transitions were collected from individual electrical traces, whose durations ranged from 10 to 15 min. For both data acquisition and analysis, the pClamp 10.5 software package (Axon) was used. Figures were prepared using ClampFit 10.7 (Axon) and Origin 8.5 (OriginLab, Northampton, MA). A logarithm likelihood ratio test was used for the single-exponential fit of the histograms³⁶. All single-channel electrical recordings were acquired at a temperature of 23 ± 1 °C.

Detection of Bs in FBS. Gibco FBS, catalog no. A3160601, was obtained from Fisher Scientific (Pittsburgh, PA). FBS was sterile-filtered using an 0.2-μm filter and kept at –80 °C for long-term storage. A fresh aliquot of this frozen serum was thawed at 4 °C and incubated at room temperature for at least 30 min before the single-channel experiment.

Reporting Summary. Further information on research design is available in the [Nature Research Reporting Summary](#) linked to this article.

Data availability. The data that support the findings of this study are available from the corresponding author upon reasonable request.

35. Guillet, V., Laphorn, A., Hartley, R.W. & Mauguen, Y. Recognition between a bacterial ribonuclease, barnase, and its natural inhibitor, barstar. *Structure* **1**, 165–176 (1993).

36. McManus, O.B. & Magleby, K.L. Kinetic states and modes of single large-conductance calcium-activated potassium channels in cultured rat skeletal muscle. *J. Physiol. (Lond.)* **402**, 79–120 (1988).

Life Sciences Reporting Summary

Nature Research wishes to improve the reproducibility of the work that we publish. This form is intended for publication with all accepted life science papers and provides structure for consistency and transparency in reporting. Every life science submission will use this form; some list items might not apply to an individual manuscript, but all fields must be completed for clarity.

For further information on the points included in this form, see [Reporting Life Sciences Research](#). For further information on Nature Research policies, including our [data availability policy](#), see [Authors & Referees](#) and the [Editorial Policy Checklist](#).

Please do not complete any field with "not applicable" or n/a. Refer to the help text for what text to use if an item is not relevant to your study. For final submission: please carefully check your responses for accuracy; you will not be able to make changes later.

▶ Experimental design

1. Sample size

Describe how sample size was determined.

The sample size was determined using standard single-channel analysis and logarithm likelihood ratio (LLR) tests.

2. Data exclusions

Describe any data exclusions.

No data were excluded from this analysis.

3. Replication

Describe the measures taken to verify the reproducibility of the experimental findings.

Experiments were performed using samples from different protein preparations. All the experiments were performed independently under similar experimental conditions on different days.

4. Randomization

Describe how samples/organisms/participants were allocated into experimental groups.

This is not relevant to our study, because of the uniform time-constant data, which followed single-exponential distributions.

5. Blinding

Describe whether the investigators were blinded to group allocation during data collection and/or analysis.

This is not relevant for the reason detailed above.

Note: all in vivo studies must report how sample size was determined and whether blinding and randomization were used.

6. Statistical parameters

For all figures and tables that use statistical methods, confirm that the following items are present in relevant figure legends (or in the Methods section if additional space is needed).

- | n/a | Confirmed |
|--------------------------|---|
| <input type="checkbox"/> | <input checked="" type="checkbox"/> The <u>exact sample size</u> (<i>n</i>) for each experimental group/condition, given as a discrete number and unit of measurement (animals, litters, cultures, etc.) |
| <input type="checkbox"/> | <input checked="" type="checkbox"/> A description of how samples were collected, noting whether measurements were taken from distinct samples or whether the same sample was measured repeatedly |
| <input type="checkbox"/> | <input checked="" type="checkbox"/> A statement indicating how many times each experiment was replicated |
| <input type="checkbox"/> | <input checked="" type="checkbox"/> The statistical test(s) used and whether they are one- or two-sided
<i>Only common tests should be described solely by name; describe more complex techniques in the Methods section.</i> |
| <input type="checkbox"/> | <input checked="" type="checkbox"/> A description of any assumptions or corrections, such as an adjustment for multiple comparisons |
| <input type="checkbox"/> | <input checked="" type="checkbox"/> Test values indicating whether an effect is present
<i>Provide confidence intervals or give results of significance tests (e.g. <i>P</i> values) as exact values whenever appropriate and with effect sizes noted.</i> |
| <input type="checkbox"/> | <input checked="" type="checkbox"/> A clear description of statistics including <u>central tendency</u> (e.g. median, mean) and <u>variation</u> (e.g. standard deviation, interquartile range) |
| <input type="checkbox"/> | <input checked="" type="checkbox"/> Clearly defined error bars in <u>all</u> relevant figure captions (with explicit mention of central tendency and variation) |

See the web collection on [statistics for biologists](#) for further resources and guidance.

► Software

Policy information about [availability of computer code](#)

7. Software

Describe the software used to analyze the data in this study.

pClamp 10.7, Clampfit 10.7, and Origin 8.6

For manuscripts utilizing custom algorithms or software that are central to the paper but not yet described in the published literature, software must be made available to editors and reviewers upon request. We strongly encourage code deposition in a community repository (e.g. GitHub). *Nature Methods* [guidance for providing algorithms and software for publication](#) provides further information on this topic.

► Materials and reagents

Policy information about [availability of materials](#)

8. Materials availability

Indicate whether there are restrictions on availability of unique materials or if these materials are only available for distribution by a third party.

All the materials are readily available from all the authors.

9. Antibodies

Describe the antibodies used and how they were validated for use in the system under study (i.e. assay and species).

No antibodies were used in this work.

10. Eukaryotic cell lines

a. State the source of each eukaryotic cell line used.

No eukaryotic cell lines were used in this work.

b. Describe the method of cell line authentication used.

No such authentication was used.

c. Report whether the cell lines were tested for mycoplasma contamination.

No such test was needed.

d. If any of the cell lines used are listed in the database of commonly misidentified cell lines maintained by [ICLAC](#), provide a scientific rationale for their use.

No commonly misidentified cell lines were used.

► Animals and human research participants

Policy information about [studies involving animals](#); when reporting animal research, follow the [ARRIVE guidelines](#)

11. Description of research animals

Provide all relevant details on animals and/or animal-derived materials used in the study.

No animals were used.

Policy information about [studies involving human research participants](#)

12. Description of human research participants

Describe the covariate-relevant population characteristics of the human research participants.

This study did not involve human research participants.